# Nonclassical Exciton Diffusion in Monolayer math xmlns="http://www.w3.org/1998/Math/MathML" display="inline">mrow>msub>mrow>mi>WSe/mi>/mrow >mrow>mn>2/mn>/mrow>/msub>/mrow>/math>

Koloman Wagner, Jonas Zipfel, Roberto Rosati, Edith Wietek, Jonas D. Ziegler, Samuel Brem, Raül Perea-Causín, Takashi Taniguchi, Kenji Watanabe, Mikhail M. Glazov, Ermin Malic, and Alexey Chernikov

Phys. Rev. Lett. **127**, 076801 — Published 9 August 2021

DOI: 10.1103/PhysRevLett.127.076801

# Nonclassical Exciton Diffusion in Monolayer $WSe_2$

Koloman Wagner,[1] Jonas Zipfel,[1,2] Roberto Rosati,[3] Edith Wietek,[1] Jonas D. Ziegler,[1] Samuel Brem,[3] Raül Perea-Causín,[4] Takashi Taniguchi,[5] Kenji Watanabe,[6] Mikhail M. Glazov,[7] Ermin Malic,[4,3] and Alexey Chernikov[1,8,*]

[1] *Department of Physics, University of Regensburg, Regensburg D-93053, Germany*
[2] *Molecular Foundry, Lawrence Berkeley National Laboratory, Berkeley, California 94720, USA*
[3] *Department of Physics, Philipps-Universität Marburg, Renthof 7, D-35032 Marburg, Germany*
[4] *Department of Physics, Chalmers University of Technology, Fysikgården 1, 41258 Gothenburg, Sweden*
[5] *International Center for Materials Nanoarchitectonics, National Institute for Materials Science, Tsukuba, Ibaraki 305-004, Japan*
[6] *Research Center for Functional Materials, National Institute for Materials Science, Tsukuba, Ibaraki 305-004, Japan*
[7] *Ioffe Institute, 194021 Saint Petersburg, Russian Federation*
[8] *Institute for Applied Physics, Dresden University of Technology, Dresden, 01187, Germany*

We experimentally demonstrate time-resolved exciton propagation in a monolayer semiconductor at cryogenic temperatures. Monitoring phonon-assisted recombination of dark states, we find a highly unusual case of exciton diffusion. While at 5 K the diffusivity is intrinsically limited by acoustic phonon scattering, we observe a pronounced *decrease* of the diffusion coefficient with increasing temperature, far below the activation threshold of higher-energy phonon modes. This behavior corresponds neither to well-known regimes of semi-classical free-particle transport nor to the thermally activated hopping in systems with strong localization. Its origin is discussed in the framework of both microscopic numerical and semi-phenomenological analytical models illustrating the observed characteristics of nonclassical propagation. Challenging the established description of mobile excitons in monolayer semiconductors, these results open up avenues to study quantum transport phenomena for excitonic quasiparticles in atomically-thin van der Waals materials and their heterostructures.

Correlated motion of the Coulomb-bound electron-hole pairs, commonly known as excitons [1, 2], represents a vibrant field of research. From their electronic constituents excitons naturally inherit the ability to propagate through the crystal [3, 4]. Moreover, optically active excitons can directly visualize transport phenomena and possess emerging properties associated with interacting, composite bosons [5], including discussions of superfluidity [6, 7], condensation [8], phonon wind [9], and ring formation [10]. Particularly interesting in this context are layered two-dimensional (2D) materials [11] such as semiconducting transition-metal dichalcogenides (TMDCs) [12–15]. As monolayers they host robust exciton states with high binding energies [16, 17] and the possibility to carry spin-valley information quanta [18–20]. The excitons in TMDCs have been shown to be mobile [21–28], guided by gradients [29–31], exhibit nonlinear diffusion [32–37], strain-dependence [38], as well as intriguing propagation in heterostructures [39–42].

In general, systems hosting mobile excitons such as TMDCs fall into two main categories, exhibiting either semi-classical free-particle transport [43–45] or hopping between localization sites [46, 47]. These mechanisms are typical for Wannier-Mott excitons with spatially extended wavefunctions in inorganic semiconductors and tightly bound Frenkel-like states in molecular crystals, respectively. Excitons in TMDC monolayers, however, present a particularly interesting, intermediate case. They uniquely combine the characteristics of the two descriptions, with wavefunctions being delocalized across many unit cells but also exhibiting high binding energies [17]. This duality is expected to manifest itself prominently in the exciton transport behavior, including potential emergence of quantum interference phenomena [48–52]. Despite much progress, however, only little is known regarding the appropriate picture for the exciton propagation in monolayer semiconductors, currently based on the assumption of a purely semi-classical framework [22, 24, 28, 30, 32, 33, 36, 37, 53].

Here, we address the question of the fundamental description of mobile excitons in 2D TMDCs, demonstrating the unusual nature of the exciton diffusion in these systems. In the experiments, we take advantage of dark excitons in hBN-encapsulated $WSe_2$ monolayers with suppressed long-range disorder [26]. In contrast to bright excitons with picosecond lifetimes [54], dark states live up to 100's of ps [55, 56] and allow us to study them under thermal equilibrium conditions. Dark exciton emission is monitored through phonon-assisted recombination channels [57–63] via time- and spatially-resolved microscopy at cryogenic temperatures after weak, strictly resonant excitation of the bright state. Importantly, the characteristic spectral shape of the phonon sidebands (PSBs) [4, 58, 61] allows for an independent evaluation of the exciton temperature and scattering rates, making it possible to extract key parameters governing exciton propagation from experiments.

At the lowest studied temperature of 5 K, we detect linear diffusion with a coefficient of $2.4 \pm 0.5\,\mathrm{cm}^2/\mathrm{s}$, essentially limited by the exciton-phonon coupling. As the

temperature increases, we observe an unusually strong *decrease* already in the low-temperature range of 4 to 30 K, far below activation threshold of high-energy phonons. Under these conditions, the observations agree neither with the semi-classical free-particle description nor with thermally activated hopping. These conclusions are further supported by quantitative analysis involving experimentally determined scattering rates as well as many-body calculations of the spatio-temporal exciton dynamics. In view of the recently predicted quantum interference phenomena for TMDC monolayers [52], it allows us to experimentally demonstrate an interesting scenario that requires nonclassical contributions to the exciton transport.

The studied hBN-encapsulated $WSe_2$ monolayers were obtained by mechanical exfoliation and stamping [64] of bulk crystals ($WSe_2$ from "HQgraphene", hBN from NIMS) onto $SiO_2$/Si substrates (see Supplemental Material [65]). For the measurements the samples were placed in a microscopy cryostat. We used a 80 MHz, 140 fs-pulsed Ti:sapphire as excitation source, tuned into resonance with the bright exciton $X_0$ at 1.726 eV to minimize excess energy and avoid contributions of unbound electron-hole pairs. The incident light was focused to a spot with about 1 $\mu$m diameter. The emission was collected from a lateral cross-section and guided through an imaging spectrometer equipped with a mirror and a grating to provide spatial and spectral resolutions, respectively. We employed a streak camera for time-resolved detection and a CCD-sensor for time-integrated signals, also see Refs. [28, 33].

The optical fingerprints used to monitor dark excitons in $WSe_2$ monolayer are schematically illustrated in Fig. 1 (a). The short-lived, bright exciton transition ($K-K$) is denoted by the respective valence and conduction band valleys of the empty and filled electron states that form the exciton. The schematic and the notation are chosen from the $K$ valley perspective and apply equally for $K'$. After optical injection, bright excitons rapidly redistribute toward lower-lying states [55, 62, 91]. These are commonly labeled as *dark excitons* [55] due to strongly suppressed light-matter coupling from either non-zero spin (*intra*-valley $K-K$ triplets) or large center-of-mass momentum (*inter*-valley $K-K'$ singlets).

While being essentially dark in absorption, these states can be detected in photoluminescence (PL) at sufficiently low temperatures [17]. Intra-valley triplets couple weakly to light via out-of-plane-polarization [56, 92] and are observed with large collection apertures. They give rise to the prominent $X^D_{\mathrm{intra}}$ transition in the PL spectrum at $T = 5$ K, presented in Fig. 1 (b). In addition, they couple to the in-plane polarization through a phonon-assisted process [59, 60, 63] leading to the emergence of the $P_{\mathrm{intra}}$ sideband, indicated in Figs. 1 (a) and (b). Similarly, inter-valley $K-K'$ singlets recombine under emission of zone-edge phonons [61–63] and exhibit PL labeled as $P_{\mathrm{inter}}$, while their direct recombination is forbidden due to momentum conservation. Additional, weak signatures stem largely from the higher order PSBs below $P_{\mathrm{intra}}$, a feature attributed to the $K-\Lambda$ sideband at about $-50$ meV [61, 62], nearly negligible PL from negative trions ($-31$ and $-38$ meV) as well as a peak at $-35$ meV, consistent with Refs. [59, 60, 63].

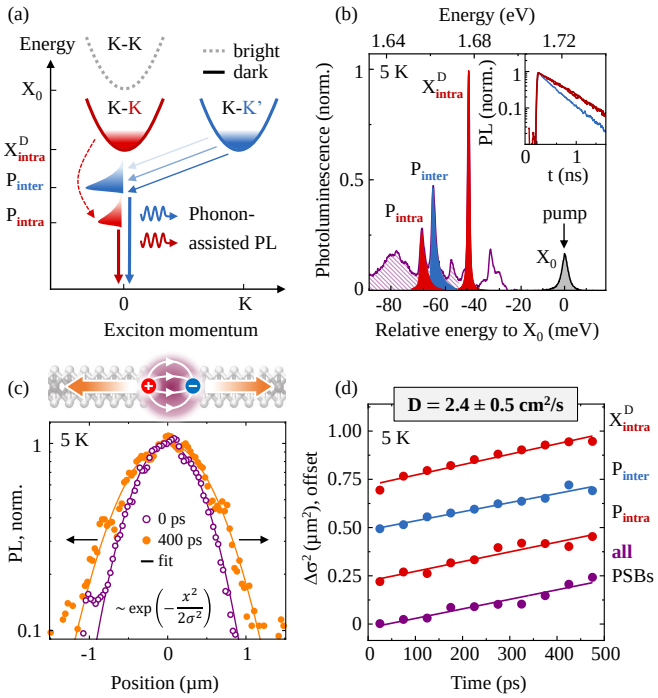


FIG. 1. (a) Schematic illustration of the relevant phonon-assisted emission of dark excitons in $WSe_2$. (b) Typical luminescence spectrum of hBN-encapsulated $WSe_2$ monolayer at $T = 5$ K, after resonant excitation of $X_0$. Colored areas schematically indicate individual components. Corresponding PL transients are presented in the inset. (c) Representative spatially-resolved profiles of the dark exciton PSBs at 0 and 400 ps after resonant excitation of $X_0$. (d) Mean squared displacement of the individually measured PL signatures as function of time. Data are vertically offset for clarity.

Importantly, all dark states are long-lived with population lifetimes $\tau_X$ of 500 and 800 ps for $P_{\mathrm{inter}}$ and $P_{\mathrm{intra}}$ ($X^D_{\mathrm{intra}}$), respectively, as illustrated in the inset of Fig. 1 (b) (also see Supplemental Material [65]). Following resonant excitation of the bright state, relaxation and cooling of dark excitons occur on much shorter timescales, during the first 10's of ps [62]. During their lifetimes of many 100's of ps, these excitons should be thus thermally equilibrated within their respective intra- and inter-valley subsets.

Representative profiles of the spatially-resolved dark state emission are presented in Fig. 1 (c) for 0 and 400 ps after the excitation at $T = 5$ K. They illustrate broadening of the spatial exciton distribution over time. The

employed excitation density of 50 nJ cm$^{-2}$ corresponds to the linear regime with the estimated electron-hole pair density of several $10^{10}$ cm$^{-2}$ per pulse. For the quantitative analysis we fit the PL profiles with a Gauss function, $\propto \exp[-x^2/2\sigma^2(t)]$, where $x$ is the coordinate along the detected cross-section. From this procedure we extract time-dependent change of the variance $\Delta\sigma^2(t) = \sigma^2(t) - \sigma^2(0)$, commonly labeled as the mean squared displacement. Corresponding values, obtained from the individual, spectrally filtered emission features of the dark states, are presented in Fig. 1 (d). All of them exhibit very similar behavior with the linear increase of $\Delta\sigma^2$ over time being a clear hallmark of diffusive propagation [11]. From $\Delta\sigma^2(t) = 2Dt$ we extract an average diffusion coefficient $D = 2.4 \pm 0.5\,\mathrm{cm}^2/\mathrm{s}$, corresponding to diffusion lengths $\sqrt{2D\tau_X}$ on the order of 0.5 $\mu$m.

According to the semi-classical description [44], the diffusion coefficient is determined by the total mass $M_X$ (that is about 0.75 of the free electron mass $m_0$ for dark excitons in $WSe_2$ [93]), temperature $T$, and the scattering rate $\tau_s^{-1}$:

$$D = \frac{k_B T \tau_s}{M_X}, \tag{1}$$

where $k_B$ denotes the Boltzmann constant. Ideally, the primary mechanism limiting the diffusion at low temperatures is the quasielastic exciton scattering with long-wavelength acoustic phonons. The corresponding rate scales linearly with the temperature and is expected to yield a temperature-independent, constant diffusivity for the purely semi-classical behavior [52]. To elucidate the nature of the exciton transport it is thus necessary to gain independent access to both diffusion coefficient and scattering rate $\tau_s^{-1}$ as functions of the exciton temperature. As we demonstrate in the following, the rates and the temperatures are directly obtained from spectrally-resolved, characteristic PSB profiles. They also allow us to confirm the equilibrated state of the photoexcited exciton system.

PL spectra in the temperature range between 5 and 50 K are presented in Figs. 2 (a) and (b) for the PSBs and the $X^D_{intra}$ peak, respectively. In order to fulfill both momentum and energy conservation, the direct radiative transition is only allowed for vanishing momenta and near-zero kinetic energies. It results in a fully symmetric $X^D_{\mathrm{intra}}$ peak that motivates the use of a Voigt profile with a temperature-dependent linewidth $\Gamma$ for analysis. In contrast to that, recombination via phonon-assisted emission can involve excitons with arbitrary large center-of-mass momenta. This yields the typically asymmetric shape of the sidebands, directly reflecting the exciton distribution in momentum space [4, 94, 95], as illustrated in Fig. 1 (a). To fit the observed PSBs we thus convolute a Lorentzian peak with an exponential high-energy flank $\propto \exp[-E/k_B T_X]$ (see Supplemental Material [65]). The

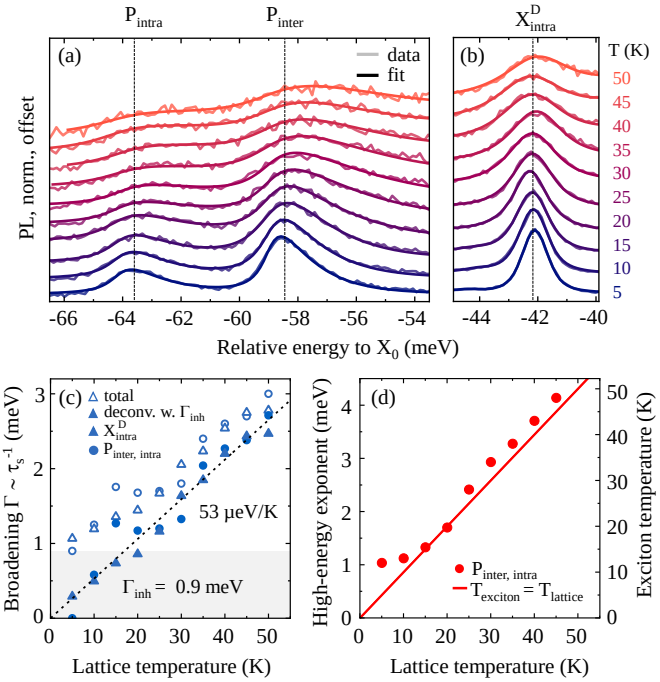


FIG. 2. (a) PL spectra of dark exciton PSBs after resonant, pulsed excitation. (b) PL spectra of the intra-valley dark exciton zero-phonon line. (c) Extracted symmetric peak broadening component (full-width-at-half-maximum) representing temperature-dependent scattering rate. (d) High-energy exponent representing the exciton temperature.

symmetric broadening then accounts for the scattering rate $\tau_s^{-1}$ and the asymmetric flank represents the exciton distribution in kinetic energy, corresponding to an effective temperature $T_X$.

As shown in Figs. 2 (a) and (b), this choice of the fit functions describes the data very well, allowing for a meaningful extraction of the parameters. Temperature-dependent broadening is presented in Fig. 2 (c) as both total and deconvoluted linewidths. For the latter we assume an additional, constant broadening of 0.9 meV to account for residual, spatially-extended inhomogeneities. The observed linear increase of the linewidth with a coefficient of 53 $\mu$eV/K is characteristic for quasielastic scattering with phonons from the linear acoustic branch [96–98] (see Supplemental Material [65] for additional discussion). In this case, each phonon-scattering event randomly changes the propagation direction of the exciton wavepacket. The *optical phase* scattering rate determining the spectral broadening is then equal to that for *momentum* scattering governing the diffusion in Eq. (1). Moreover, the broadening obtained from the symmetric component of the PSBs is nearly identical to that of the $X^D_{\mathrm{intra}}$ peak, supporting the consistency of the applied model. Finally, the extracted exciton temperature presented in Fig. 2 (d) corresponds to that of the lattice with only small deviations.

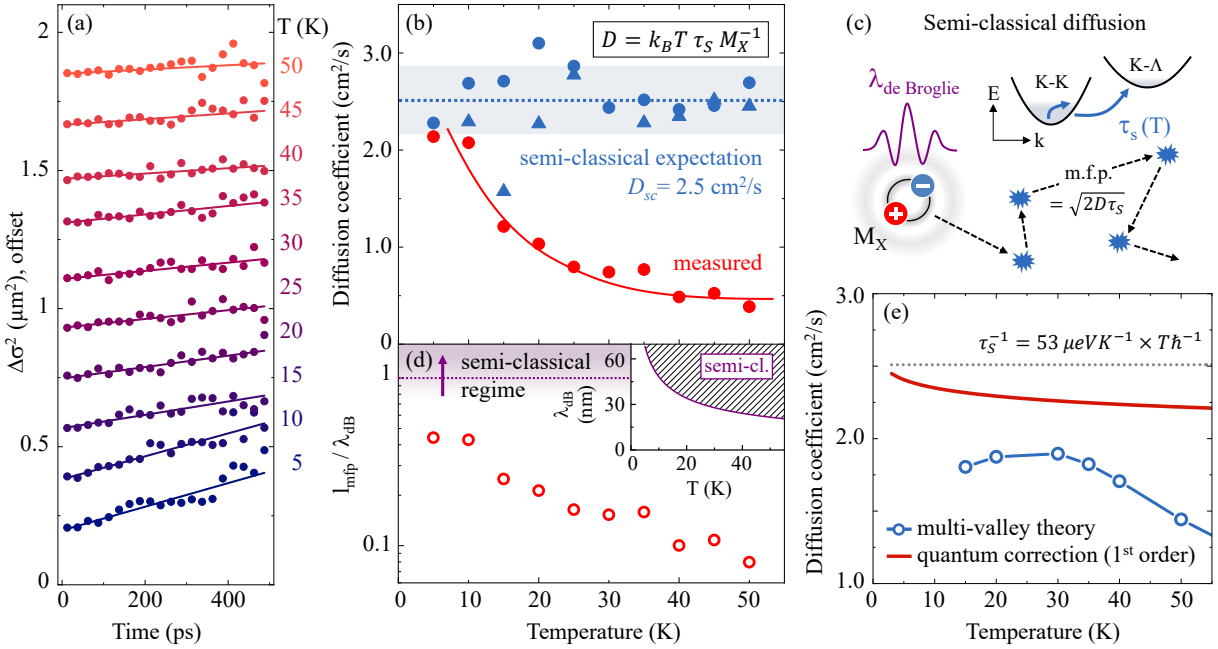


FIG. 3. (a) Transient mean squared displacement of the spatial exciton distribution for temperatures between 5 and 50 K. Data are vertically offset for clarity. (b) Measured diffusion coefficients in comparison to the semi-classical expectation from Eq.(1) based on the measured scattering rates, Fig. 2 (c). Shaded area and the solid line are guides-to-the-eye. (c) Illustration of the semi-classical exciton propagation and scattering via thermally-activated phonon absorption. (d) Temperature-dependent ratio of the mean free path corresponding to measured diffusion coefficients and the de Broglie wavelength of the excitons. Absolute values for the latter are given in the inset. (e) Exciton diffusivity calculated using a microscopic multi-valley model in a semi-classical framework and the influence of quantum-corrections.

To illustrate temperature-dependent diffusion, time-dependent expansion of the spatially-resolved PL profiles is presented in Fig. 3 (a) for a series of temperatures up to 50 K. Here, we detect the accumulated signal of all sidebands taking advantage of enhanced signal-to-noise ratio and spectrally-independent diffusion coefficients (c.f. Fig. 1). The extracted diffusivity is shown in Fig. 3 (b) as a function of temperature. At lowest temperatures the measured values are close to the semi-classical expectation $D_{sc} = 2.5\,\mathrm{cm}^2/\mathrm{s}$ using the measured broadening coefficient of $53\,\mu\mathrm{eV/K}$ and Eq. (1). As the temperature increases, we do not observe any thermally activated increase of diffusion that would otherwise point to hopping [47] or defect-assisted scattering [99, 100]. Instead, we find a pronounced *decrease* of the diffusivity already during the first 10's of K.

This peculiar observation strongly contrasts the expectation of a constant diffusivity from the semi-classical model, Eq.(1), using independently determined scattering rates, Fig. 2 (c), shown for direct comparison. Importantly, the general description via. Eq.(1) does not depend on a specific origin of the scattering. We further emphasize the absence of non-equilibrium effects due to the long time-scales in our observations, far beyond the initial relaxation during the first 10's of ps [62]. Finally, our findings are robust, confirmed using a sample in the neutral-doping regime, and do not depend on the excitation density (see Supplemental Material [65]). The latter allows us to exclude non-linearities, such as bimolecular processes [33, 101] or phonon-wind effects [35, 102].

The observed inadequacy of the semi-classical description can be rationalized in view of the formal applicability limit, known as the Ioffe-Regel criterion [103]. In the semi-classical picture, schematically illustrated in Fig. 3 (c), the exciton diffusion is dictated by temperature and scattering rate $\tau_s^{-1}$. The model is expected to break down when the mean-free-path $l_{\mathrm{mfp}} = \sqrt{2D\tau_s}$ of the particle becomes similar or smaller than the wavepacket size characterized by the de Broglie wavelength $\lambda_{\mathrm{dB}} = \sqrt{2}\pi\hbar(M_X k_B T)^{-1/2}$. From scattering rates in Fig. 2 (c) we indeed obtain $l_{\mathrm{mfp}} \approx \lambda_{\mathrm{dB}}$ for all studied temperatures. We also present the ratio between $l_{\mathrm{mfp}}$, extracted from measured diffusion coefficients under the assumption of Eq.(1), and $\lambda_{\mathrm{dB}}$ in Fig. 3 (d). This ratio decreases far below unity at elevated temperatures, further illustrating the inconsistency of the semi-classical description. Moreover, due to the similarity of the key exciton parameters and scattering rates, the above considerations should apply for other TMDC monolayers as well.

It is thus instructive to consider current theoretical understanding of the exciton transport in 2D TMDCs both in a semi-classical framework with a more comprehensive description of exciton bandstructure and from the perspective of quantum corrections. For this purpose, the re-

sults of the calculations for the exciton diffusivity in thermal equilibrium are presented in Fig. 3 (e). In the multi-valley approach we use a model Hamiltonian in the excitonic basis, including carrier–light, carrier–phonon, and carrier–carrier interactions to set up equations of motion for the excitons [36, 38, 62]. The required input parameters for monolayer $WSe_2$ are taken from first-principle studies [93, 104]. The diffusion coefficient is extracted from the spatio-temporal evolution of the excitons in the semi-classical approximation neglecting exciton-exciton mechanisms [36–38]. The model takes explicitly into account both a realistic multi-valley bandstructure of $WSe_2$ and the exciton-phonon coupling beyond the long-wavelength acoustic branches. In particular, we include thermal activation of higher-energy phonon absorption that leads to additional inter-valley scattering for excitons, schematically illustrated in Fig. 3 (c). At low temperatures we find an essentially constant value of the diffusion coefficient, close to the experimental result at 5 K and the semi-classical estimation via Eq. (1). Only above about 30 K the model predicts a small decrease of the diffusivity. This onset depends on the energy of the phonons involved in the intervalley scattering and, most importantly, is always accompanied by a non-linear increase of the linewidth (cf. Supplemental Material [65] and Ref. [98]).

First-order quantum corrections to a simplified semi-classical picture of constant diffusivity are illustrated in Fig. 3 (e). Recently developed for 2D TMDCs [52], the calculations are adapted for the $WSe_2$ monolayer by using the exciton mass and the sound velocity of $0.75\,m_0$ and 3.3 km/s, respectively. The model accounts perturbatively for quantum interference effects in the exciton transport. Constructive interference can arise between clock- and counterclockwise propagation of exciton wave packets through closed loops, leading to an effective localization of excitons (also see Supplementary Material [65]). For quasielastic exciton-phonon interaction [52], the specific interplay between the loss of the *relative* phase in the loop and momentum scattering results in an initial *decrease* of the effective diffusivity with increasing temperature. Interestingly, the functional form of the quantum corrections and their temperature dependence indeed resemble experimental observations. However, the magnitude of the measured effect is almost an order of magnitude higher. It follows that while nonclassical contributions to the exciton diffusion are clearly necessary, further development of the theory beyond the commonly studied first order in $\hbar/(k_B T \tau_s)$ quantum corrections is required.

In conclusion, we have explored the nature of the exciton transport in monolayer semiconductors via transient microscopy at cryogenic temperatures. The excitons are found to exhibit neither the characteristic behavior of diffusive free particle propagation nor that of thermally activated hopping between localized states. Measured diffusion coefficients strongly deviate from the semi-classical expectation of a temperature-independent diffusivity based on independently obtained momentum scattering rates. Instead, we find evidence for nonclassical contributions playing a key role, consistent with comparable scales for the free propagation and de Broglie lengths. The obtained results should be relevant for optoelectronic devices based on mobile optical excitations in 2D materials and provide a solid platform to understand exciton propagation in more complex heterostructures that involve monolayers as building blocks. The observed unusual behavior in the exciton diffusion highlights van der Waals monolayer semiconductors as a particularly promising platform to merge the rich field of quantum transport phenomena with the physics of composite excitonic quasiparticles.

* alexey.chernikov@tu-dresden.de


[1] J. Frenkel, Phys. Rev. **37**, 17 (1931).
[2] E. F. Gross and N. A. Karrjew, Dokl. Akad. Nauk SSSR **84**, 471 (1952).
[3] E. L. Ivchenko, *Optical spectroscopy of semiconductor nanostructures* (Alpha Science, Harrow England, 2005).
[4] C. Klingshirn, *Semiconductor Optics*, 3rd ed. (Springer, Berlin Heidelberg New York, 2007).
[5] H. Haug and S. W. Koch, *Quantum theory of the optical and electronic properties of semiconductors*, 5th ed. (World Scientific, Singapore, 2009).
[6] A. Mysyrowicz, E. Benson, and E. Fortin, Phys. Rev. Lett. **77**, 896 (1996).
[7] E. Benson, E. Fortin, and A. Mysyrowicz, Solid State Commun. **101**, 313 (1997).
[8] S. A. Moskalenko and D. W. Snoke, *Bose-Einstein condensation of excitons and biexcitons* (Cambridge University Press, 2005).
[9] S. Tikhodeev, G. Kopelevich, and N. Gippius, Phys. status solidi **206**, 45 (1998).
[10] L. V. Butov, L. S. Levitov, A. V. Mintsev, B. D. Simons, A. C. Gossard, and D. S. Chemla, Phys. Rev. Lett. **92**, 117404 (2004).
[11] N. S. Ginsberg and W. A. Tisdale, Annu. Rev. Phys. Chem. **71**, 1 (2020).
[12] J. Wilson and A. Yoffe, Adv. Phys. **18**, 193 (1969).
[13] K. S. Novoselov, D. Jiang, F. Schedin, T. J. Booth, V. V. Khotkevich, S. V. Morozov, and A. K. Geim, Proc. Natl. Acad. Sci. USA **102**, 10451 (2005).
[14] K. F. Mak, C. Lee, J. Hone, J. Shan, and T. F. Heinz, Phys. Rev. Lett. **105**, 136805 (2010).
[15] A. Splendiani, L. Sun, Y. Zhang, T. Li, J. Kim, C.-Y. Chim, G. Galli, and F. Wang, Nano Lett. **10**, 1271 (2010).
[16] J. Xiao, M. Zhao, Y. Wang, and X. Zhang, Nanophotonics **6**, 1309 (2017).
[17] G. Wang, A. Chernikov, M. M. Glazov, T. F. Heinz, X. Marie, T. Amand, and B. Urbaszek, Rev. Mod. Phys. **90**, 021001 (2018).
[18] X. Xu, W. Yao, D. Xiao, and T. F. Heinz, Nat. Phys. **10**, 343 (2014).

[19] H. Yu, X. Cui, X. Xu, and W. Yao, Natl. Sci. Rev. **2**, 57 (2015).
[20] M. M. Glazov and L. E. Golub, Phys. Rev. Lett. **125**, 157403 (2020).
[21] N. Kumar, Q. Cui, F. Ceballos, D. He, Y. Wang, and H. Zhao, Phys. Rev. B **89**, 125427 (2014).
[22] T. Kato and T. Kaneko, ACS Nano **10**, 9687 (2016).
[23] L. Yuan, T. Wang, T. Zhu, M. Zhou, and L. Huang, J. Phys. Chem. Lett. **8**, 3371 (2017).
[24] F. Cadiz, C. Robert, E. Courtade, M. Manca, L. Martinelli, T. Taniguchi, K. Watanabe, T. Amand, A. C. H. Rowe, D. Paget, B. Urbaszek, and X. Marie, Appl. Phys. Lett. **112**, 152106 (2018).
[25] Y. Fu, D. He, J. He, A. Bian, L. Zhang, S. Liu, Y. Wang, and H. Zhao, Adv. Mater. Interfaces , 1901307 (2019).
[26] A. Raja, L. Waldecker, J. Zipfel, Y. Cho, S. Brem, J. D. Ziegler, M. Kulig, T. Taniguchi, K. Watanabe, E. Malic, T. F. Heinz, T. C. Berkelbach, and A. Chernikov, Nat. Nanotechnol. **14**, 832 (2019).
[27] S. Z. Uddin, H. Kim, M. Lorenzon, M. Yeh, D.-H. Lien, E. S. Barnard, H. Htoon, A. Weber-Bargioni, and A. Javey, ACS Nano **14**, 13433 (2020).
[28] J. Zipfel, M. Kulig, R. Perea-Causín, S. Brem, J. D. Ziegler, R. Rosati, T. Taniguchi, K. Watanabe, M. M. Glazov, E. Malic, and A. Chernikov, Phys. Rev. B **101**, 115430 (2020).
[29] D. F. Cordovilla Leon, Z. Li, S. W. Jang, C.-H. Cheng, and P. B. Deotare, Appl. Phys. Lett. **113**, 252101 (2018).
[30] V. Shahnazaryan, O. Kyriienko, and H. Rostami, Phys. Rev. B **100**, 165303 (2019).
[31] S. Hao, M. Z. Bellus, D. He, Y. Wang, and H. Zhao, Nanoscale Horizons **5**, 139 (2020).
[32] S. Mouri, Y. Miyauchi, M. Toh, W. Zhao, G. Eda, and K. Matsuda, Phys. Rev. B **90**, 155449 (2014).
[33] M. Kulig, J. Zipfel, P. Nagler, S. Blanter, C. Schüller, T. Korn, N. Paradiso, M. M. Glazov, and A. Chernikov, Phys. Rev. Lett. **120**, 207401 (2018).
[34] J. Wang, Y. Guo, Y. Huang, H. Luo, X. Zhou, C. Gu, and B. Liu, Appl. Phys. Lett. **115**, 131902 (2019).
[35] M. M. Glazov, Phys. Rev. B **100**, 045426 (2019).
[36] R. Perea-Causín, S. Brem, R. Rosati, R. Jago, M. Kulig, J. D. Ziegler, J. Zipfel, A. Chernikov, and E. Malic, Nano Lett. **19**, 7317 (2019).
[37] R. Rosati, R. Perea-Causín, S. Brem, and E. Malic, Nanoscale **12**, 356 (2020).
[38] R. Rosati, S. Brem, R. Perea-Causín, R. Schmidt, I. Niehues, S. Michaelis de Vasconcellos, R. Bratschitsch, and E. Malic, 2D Mater. **8**, 015030 (2021).
[39] P. Rivera, K. L. Seyler, H. Yu, J. R. Schaibley, J. Yan, D. G. Mandrus, W. Yao, and X. Xu, Science (80-. ). **351**, 688 (2016).
[40] E. V. Calman, M. M. Fogler, L. V. Butov, S. Hu, A. Mishchenko, and A. K. Geim, Nat. Commun. **9**, 1895 (2018).
[41] D. Unuchek, A. Ciarrocchi, A. Avsar, K. Watanabe, T. Taniguchi, and A. Kis, Nature **560**, 340 (2018).
[42] L. Yuan, B. Zheng, J. Kunstmann, T. Brumme, A. B. Kuc, C. Ma, S. Deng, D. Blach, A. Pan, and L. Huang, Nat. Mater. **19**, 617 (2020).
[43] L. M. Smith, D. R. Wake, J. P. Wolfe, D. Levi, M. V. Klein, J. Klem, T. Henderson, and H. Morkoç, Phys. Rev. B **38**, 5788 (1988).
[44] J. Erland, B. S. Razbirin, K.-H. Pantke, V. G. Lyssenko, and J. M. Hvam, Phys. Rev. B **47**, 3582 (1993).
[45] S. Grosse, R. Arnold, G. von Plessen, M. Koch, J. Feldmann, V. M. Axt, T. Kuhn, R. Rettig, and W. Stolz, Phys. status solidi **204**, 147 (1997).
[46] P. W. Anderson, Phys. Rev. **109**, 1492 (1958).
[47] O. V. Mikhnenko, P. W. M. Blom, and T.-Q. Nguyen, Energy Environ. Sci. **8**, 1867 (2015).
[48] E. L. Ivchenko, G. E. Pikus, B. S. Razbirin, and A. I. Starukhin, JETP **45**, 1172 (1977).
[49] B. Altshuler and A. Aronov, *Electron-Electron Interactions in Disordered Systems*, edited by A. E. and M. and Pollak (North Holland, Amsterdam, 1985).
[50] P. I. Arseev and A. B. Dzyubenko, J. Exp. Theor. Phys. **87**, 200 (1998).
[51] F. Evers and A. D. Mirlin, Rev. Mod. Phys. **80**, 1355 (2008).
[52] M. M. Glazov, Phys. Rev. Lett. **124**, 166802 (2020).
[53] M. G. Harats, J. N. Kirchhof, M. Qiao, K. Greben, and K. I. Bolotin, Nat. Photonics **14**, 324 (2020).
[54] C. Robert, R. Picard, D. Lagarde, G. Wang, J. P. Echeverry, F. Cadiz, P. Renucci, A. Högele, T. Amand, X. Marie, I. C. Gerber, and B. Urbaszek, Phys. Rev. B **94**, 155425 (2016).
[55] X.-X. Zhang, Y. You, S. Y. F. Zhao, and T. F. Heinz, Phys. Rev. Lett. **115**, 257403 (2015).
[56] C. Robert, T. Amand, F. Cadiz, D. Lagarde, E. Courtade, M. Manca, T. Taniguchi, K. Watanabe, B. Urbaszek, and X. Marie, Phys. Rev. B **96**, 155423 (2017).
[57] J. Lindlau, C. Robert, V. Funk, J. Förste, M. Förg, L. Colombier, A. Neumann, E. Courtade, S. Shree, T. Taniguchi, K. Watanabe, M. M. Glazov, X. Marie, B. Urbaszek, and A. Högele, (2017), arXiv:1710.00988.
[58] D. Christiansen, M. Selig, G. Berghäuser, R. Schmidt, I. Niehues, R. Schneider, A. Arora, S. M. de Vasconcellos, R. Bratschitsch, E. Malic, and A. Knorr, Phys. Rev. Lett. **119**, 187402 (2017).
[59] C. Liu, H. Hong, Q. Wang, P. Liu, Y. Zuo, J. Liang, Y. Cheng, X. Zhou, J. Wang, Y. Zhao, J. Xiong, B. Xiang, J. Zhang, and K. Liu, Nanoscale **11**, 17195 (2019).
[60] Z. Li, T. Wang, C. Jin, Z. Lu, Z. Lian, Y. Meng, M. Blei, S. Gao, T. Taniguchi, K. Watanabe, T. Ren, S. Tongay, L. Yang, D. Smirnov, T. Cao, and S.-F. Shi, Nat. Commun. **10**, 2469 (2019).
[61] S. Brem, A. Ekman, D. Christiansen, F. Katsch, M. Selig, C. Robert, X. Marie, B. Urbaszek, A. Knorr, and E. Malic, Nano Lett. **20**, 2849 (2020).
[62] R. Rosati, K. Wagner, S. Brem, R. Perea-Causín, E. Wietek, J. Zipfel, J. D. Ziegler, M. Selig, T. Taniguchi, K. Watanabe, A. Knorr, A. Chernikov, and E. Malic, ACS Photonics **7**, 2756 (2020).
[63] M. He, P. Rivera, D. Van Tuan, N. P. Wilson, M. Yang, T. Taniguchi, K. Watanabe, J. Yan, D. G. Mandrus, H. Yu, H. Dery, W. Yao, and X. Xu, Nat. Commun. **11**, 618 (2020).
[64] A. Castellanos-Gomez, M. Buscema, R. Molenaar, V. Singh, L. Janssen, H. S. J. van der Zant, and G. A. Steele, 2D Mater. **1**, 011002 (2014).
[65] See Supplemental Material at [url], which includes Refs. [65]–[89], for additional experimental data, theoretical analysis, and discussion.
[66] S. J. Byrnes, (2016), arXiv:1603.02720.
[67] Y. Li, A. Chernikov, X. Zhang, A. Rigosi, H. M. Hill, A. M. van der Zande, D. A. Chenet, E.-M. Shih, J. Hone, and T. F. Heinz, Phys. Rev. B **90**, 205422 (2014).

[68] Y. You, X. Zhang, T. C. Berkelbach, M. S. Hybertsen, D. R. Reichman, and T. F. Heinz, Nat. Phys. **11**, 477 (2015).

[69] Z. Ye, L. Waldecker, E. Y. Ma, D. Rhodes, A. Antony, B. Kim, X.-X. Zhang, M. Deng, Y. Jiang, Z. Lu, D. Smirnov, K. Watanabe, T. Taniguchi, J. Hone, and T. F. Heinz, Nat. Commun. **9**, 3718 (2018).

[70] A. J. Goodman, D.-H. Lien, G. H. Ahn, L. L. Spiegel, M. Amani, A. P. Willard, A. Javey, and W. A. Tisdale, J. Phys. Chem. C **124**, 12175 (2020).

[71] J. D. Ziegler, J. Zipfel, B. Meisinger, M. Menahem, X. Zhu, T. Taniguchi, K. Watanabe, O. Yaffe, D. A. Egger, and A. Chernikov, Nano Lett. **20**, 6674 (2020).

[72] C. Robert, D. Lagarde, F. Cadiz, G. Wang, B. Lassagne, T. Amand, A. Balocchi, P. Renucci, S. Tongay, B. Urbaszek, and X. Marie, Phys. Rev. B **93**, 205423 (2016).

[73] V. Chellappan, A. L. C. Pang, S. Sarkar, Z. E. Ooi, and K. E. J. Goh, Electron. Mater. Lett. **14**, 766 (2018).

[74] J. Olivero, JQSRT **17**, 233 (1977).

[75] T. Deilmann and K. S. Thygesen, 2D Mater. **6**, 035003 (2019).

[76] E. Malic, M. Selig, M. Feierabend, S. Brem, D. Christiansen, F. Wendler, A. Knorr, and G. Berghäuser, Phys. Rev. Materials **2**, 014002 (2018).

[77] Z. Khatibi, M. Feierabend, M. Selig, S. Brem, C. Linderälv, P. Erhart, and E. Malic, 2D Mater. **6**, 015015 (2018).

[78] J. Madéo, M. K. L. Man, C. Sahoo, M. Campbell, V. Pareek, E. L. Wong, A. Al-Mahboob, N. S. Chan, A. Karmakar, B. M. K. Mariserla, X. Li, T. F. Heinz, T. Cao, and K. M. Dani, Science **370**, 1199 (2020).

[79] S. Dong, M. Puppin, T. Pincelli, S. Beaulieu, D. Christiansen, H. Hubener, C. W. Nicholson, R. P. Xian, M. Dendzik, Y. Deng, *et al.*, arXiv:2012.15328 (2020).

[80] R. Wallauer, R. Perea-Causin, L. Münster, S. Zajusch, S. Brem, J. Güdde, K. Tanimura, K. Lin, R. Huber, E. Malic, *et al.*, arXiv:2012.11385 (2020).

[81] L. E. Golub, E. L. Ivchenko, and A. A. Kiselev, J. Opt. Soc. Am. B **13**, 1199 (1996).

[82] R. Westphäling, S. Bauer, C. Klingshirn, A. Reznitstsky, and S. Verbin, J. Cryst. Growth **184-185**, 1072 (1998).

[83] S. A. Tarasenko, A. A. Kiselev, E. L. Ivchenko, A. Dinger, M. Baldauf, C. Klingshirn, H. Kalt, S. D. Baranovskii, R. Eichmann, and P. Thomas, Semicond. Sci. Technol. **16**, 486 (2001).

[84] H. Hillmer, A. Forchel, S. Hansmann, M. Morohashi, E. Lopez, H. P. Meier, and K. Ploog, Phys. Rev. B **39**, 10901 (1989).

[85] K. T. Tsen, O. F. Sankey, and H. Moroc, Appl. Phys. Lett. **57**, 1666 (1990).

[86] S. Shree, M. Semina, C. Robert, B. Han, T. Amand, A. Balocchi, M. Manca, E. Courtade, X. Marie, T. Taniguchi, K. Watanabe, M. M. Glazov, and B. Urbaszek, Phys. Rev. B **98**, 035302 (2018).

[87] V. L. Alperovich, V. M. Zaletin, A. F. Kravchenko, and A. S. Terekhov, Phys. Stat. Sol (b) **77**, 465 (1976).

[88] T. Ruf, J. Spitzer, V. F. Sapega, V. I. Belitsky, M. Cardona, and K. Ploog, Phys. Rev. B **50**, 1792 (1994).

[89] D. Gammon, S. Rudin, T. L. Reinecke, D. S. Katzer, and C. S. Kyono, Phys. Rev. B **51**, 16785 (1995).

[90] B. Jusserand, A. N. Poddubny, A. V. Poshakinskiy, A. Fainstein, and A. Lemaitre, Phys. Rev. Lett. **115**, 267402 (2015).

[91] M. Selig, G. Berghäuser, A. Raja, P. Nagler, C. Schüller, T. F. Heinz, T. Korn, A. Chernikov, E. Malic, and A. Knorr, Nat. Commun. **7**, 13279 (2016).

[92] G. Wang, C. Robert, M. M. Glazov, F. Cadiz, E. Courtade, T. Amand, D. Lagarde, T. Taniguchi, K. Watanabe, B. Urbaszek, and X. Marie, Phys. Rev. Lett. **047401**, 1 (2017).

[93] A. Kormányos, G. Burkard, M. Gmitra, J. Fabian, V. Zólyomi, N. D. Drummond, and V. Fal'ko, 2D Mater. **2**, 022001 (2015).

[94] D. Hägele, R. Zimmermann, M. Oestreich, M. R. Hofmann, W. W. Rühle, B. K. Meyer, H. Amano, and I. Akasaki, Phys. Rev. B **59**, R7797 (1999).

[95] M. Kozhevnikov, B. Ashkinadze, E. Cohen, and A. Ron, J. Lumin. **72-74**, 312 (1997).

[96] S. Rudin, T. Reinecke, and B. Segall, Phys. Rev. B **42**, 11218 (1990).

[97] G. Moody, C. Kavir Dass, K. Hao, C.-H. Chen, L.-J. Li, A. Singh, K. Tran, G. Clark, X. Xu, G. Berghäuser, E. Malic, A. Knorr, and X. Li, Nat. Commun. **6**, 8315 (2015).

[98] S. Brem, J. Zipfel, M. Selig, A. Raja, L. Waldecker, J. D. Ziegler, T. Taniguchi, K. Watanabe, A. Chernikov, and E. Malic, Nanoscale **11**, 12381 (2019).

[99] H. Hillmer, S. Hansmann, A. Forchel, M. Morohashi, E. Lopez, H. P. Meier, and K. Ploog, Appl. Phys. Lett. **53**, 1937 (1988).

[100] D. Oberhauser, K.-H. Pantke, J. M. Hvam, G. Weimann, and C. Klingshirn, Phys. Rev. B **47**, 6827 (1993).

[101] J. T. Warren, K. E. O'Hara, and J. P. Wolfe, Phys. Rev. B **61**, 8215 (2000).

[102] L. M. Smith, J. S. Preston, J. P. Wolfe, D. R. Wake, J. Klem, T. Henderson, and H. Morkoç, Phys. Rev. B **39**, 1862 (1989).

[103] L. Landau and E. Lifshitz, *Physical Kinetics* (Butterworth-Heinemann, Oxford, 1981).

[104] Z. Jin, X. Li, J. T. Mullen, and K. W. Kim, Phys. Rev. B **90**, 045422 (2014).


## ACKNOWLEDGMENTS


We thank Alexander Högele and Victor Funk for fruitful discussions as well as Christian Bäuml and Nicola Paradiso for their assistance with pre-patterned substrate preparation. Financial support by the DFG via Emmy Noether Initiative (CH 1672/1), SFB 1277 (project B05), and SFB 1083 (project B09) is gratefully acknowledged. The theoretical part of the work by R.R., S.B., R. P.-C., and E.M. was further supported by the European Union's Horizon 2020 research and innovation program under grant agreement no. 881603. The computations were enabled by resources provided by the Swedish National Infrastructure for Computing (SNIC) at C3SE and HPC2N. We acknowledge the funding provided by 2D TECH VINNOVA competence Center (Ref. 2019-00068). K. Watanabe and T.T. acknowledge support from the Elemental Strategy Initiative, conducted by the MEXT, Japan, Grant Number JPMXP0112101001, JSPS KAK-

ENHI Grant Numbers JP20H00354 and the CREST (JPMJCR15F3), JST. The development of the analytical theory by M.M.G. has been supported by RSF Project No. 19-12-00051.